Nanofibrillar Networks in Poly(ethyl methacrylate) and Its Silica Nanocomposites

Elizabeth A. Wilder,[†] Michael B. Braunfeld,[§] Hiroshi Jinnai,[||] Carol K. Hall,[†] David A. Agard,[§] and Richard J. Spontak*[,†,‡]

Departments of Chemical Engineering and Materials Science & Engineering, North Carolina State University, Raleigh, North Carolina 27695, Departments of Biochemistry & Biophysics and the Howard Hughes Medical Institute, University of California, San Francisco, California 94143, and Department of Polymer Science & Engineering, Kyoto Institute of Technology, Kyoto 606-8585, Japan

Received: April 24, 2003; In Final Form: August 12, 2003

Recent advances in polymer materials design seek to incorporate functionality, enhance existing properties, and reduce weight without compromising mechanical properties or processability. While much attention has been drawn to the development of organic/inorganic hybrid nanocomposites modified with discrete siliceous nanoparticles (such as fumed/colloidal silica or organoclays), other opportunities exist for comparably enlightened materials design. Dibenzylidene sorbitol (DBS) is a sugar derivative that is capable of self-organizing into a 3D nanofibrillar network at relatively low concentrations in a wide variety of organic solvents and polymers. In this work, we explore the morphological characteristics and properties of DBS in poly(ethyl methacrylate) (PEMA) and PEMA nanocomposites with colloidal silica. Transmission electron microscopy and microtomography reveal that the DBS molecules form highly connected networks, with nanofibrils measuring ca. 10 nm in diameter and ranging up to several hundred nanometers in length. Dynamic mechanical property analysis reveals that, while DBS has little effect on glassy PEMA, it serves to increase the elastic modulus in molten PEMA.

Introduction

Polymer nanocomposites generally refer to organic/inorganic materials designed so that the matrix consists of a macromolecule to which an inorganic nanoscale particle is physically added or in which an inorganic species is grown under tightly controlled conditions to retain nanoscale dimensions and minimize aggregation.[1,2] Incorporation of such particles provides a versatile and efficient route to multifunctional materials possessing enhanced properties such as electrical conductivity,[3,4] nonlinear optics,[5,6] mechanical toughness,[7] catalytic activity,[2] separation selectivity,[8] and magnetism.[9] In this work, we only consider those nanocomposites prepared by the addition of inorganic particles, such as fumed or colloidal silica, to a polymer matrix. Colloidal silica has been widely used in the production of polymer nanocomposites due to its ability to improve mechanical stability at elevated temperatures,[10] electrical conductivity,[11] and reverse selectivity.[12] One of the challenges that plagues nanocomposite design is the integration of new functionality without compromising the inherent properties, e.g., optical clarity, mechanical toughness, and facile processability, of the polymer matrix. Fumed silica particles, for instance, may aggregate as a polymer nanocomposite consisting of PDMS ages,[1] leading to the undesirable deterioration of optical clarity. One strategy to eliminate dispersion problems arising from inorganic nanofillers is to immobilize, and therefore stabilize, the particles within a continuous nanoscale network.

1,3:2,4-Dibenzylidene-D-sorbitol (DBS) is a derivative of the natural sugar alcohol D-glucitol[13] and can be synthesized by a condensation reaction between benzaldehyde and sorbitol.[14] In its native state, DBS is a crystalline solid with a melting point of about 220 °C.[15] This amphiphilic molecule is depicted in Scheme 1 and is often described as "butterfly-like" with a sorbitol body and two benzylidene wings. The hydrophobic phenyl rings facilitate DBS dissolution in a wide variety of organic media,[16] and, together with its ether linkages and pendant hydroxyl groups, endow DBS with a unique ability to self-organize into nanofibrils that, at surprisingly low concentrations, form a 3D nanoscale network and ultimately induce physical gelation.[17] Since the pioneering gelation studies[18,19] of DBS in organic solvents, numerous efforts have demonstrated that this low-molar-mass organic gelator (LMOG) can form stable networks in, and consequently gel, a wide variety of macromolecules including polyolefins such as isotactic polypropylene (iPP),[20] polyethers such as poly(propylene glycol) (PPG)[21−23] and poly(ethylene glycol) (PEG),[24] and silicones such as poly(dimethylsiloxane) (PDMS).[25] Moreover, DBS has been found to gel small-molecule liquid crystals[26] and block copolymers[27,28] derived from PPG, PEG, and/or PDMS, all of which can exhibit mesomorphic behavior on their own. Since DBS can promote gelation in some organic systems at concentrations as low as 0.1 wt %,[29] it is particularly attractive for technologies requiring uncompromised physical and/or chemical properties of a polymer melt in a thermally reversible and thixotropic elastic solid.

SCHEME 1

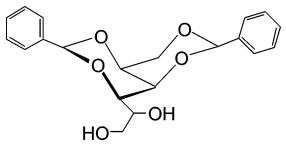

* Corresponding author. E-mail: Rich_Spontak@ncsu.edu.
† Department of Chemical Engineering, North Carolina State University.
‡ Department of Materials Science & Engineering, North Carolina State University.
§ University of California.
|| Kyoto Institute of Technology.

10.1021/jp035113u CCC: $25.00
Published on Web 09/27/2003

While the ability of DBS to self-organize into nanofibrils and nanofibrillar networks in polymer melts is now reasonably well-established, the ongoing development of polymers with a nanoscopic skeletal network opens up two new possible applications for DBS. In the first, a crystalline DBS network could endow amorphous polymers with greater load-bearing ability. This improvement is expected to be of little consequence in glassy polymers below their glass transition temperature (T_g), but it should be beneficial above T_g in the melt. Another use of DBS is as a stabilizing agent for other additives, such as nanoparticles. In this case, the DBS network is envisaged to immobilize the nanoparticles and prevent their long-term aggregation. Since the network dissolves at temperatures far below the melting point of DBS, polymer nanocomposites incorporating DBS could be melt- or solvent-processed without degrading the polymer matrix. In this work, we explore the utility of forming DBS networks in an optically clear acrylic polymer with and without colloidal silica (CS) nanoparticles. The morphological characteristics of the resultant networks, as well as their impact on mechanical properties, are assessed to identify the conditions under which the added DBS serves to improve properties without compromise.

Experimental Section

Materials. Poly(ethyl methacrylate) (PEMA) with a molecular weight of ~280 000 was purchased from Scientific Polymer Products, Inc (Ontario, NY) and used without further purification. The DBS was kindly supplied by Milliken Chemicals (Spartanburg, SC), and reagent-grade acetone was purchased from Fisher Scientific (Suwanee, GA). The CS nanoparticles, having a reported diameter of 20 nm, were provided as a suspension in methyl ethyl ketone (MEK) by Nissan Chemical Houston Corporation (Pasadena, TX).

Methods. Films of PEMA with and without various concentrations of DBS and/or CS were prepared by first dissolving 1−2 g of PEMA and a corresponding amount of DBS in approximately 20 mL of acetone. To generate a nanocomposite of given composition, a predetermined amount of the CS/MEK suspension was also added at this point. While being constantly stirred, the PEMA/DBS and PEMA/DBS/CS suspensions were heated to approximately 70 °C for 30 min and then permitted to sit quiescently overnight to ensure that the PEMA and DBS powders fully dissolved. These media were poured into Teflon molds and placed in an oven maintained at 65 °C (the T_g of the PEMA is reported to be about 63 °C according to the manufacturer) for ~2 h, followed by an additional hour at 75 °C to ensure complete evaporation of the acetone and MEK without promoting thermal degradation. The resultant PEMA/DBS and PEMA/DBS/CS films were carefully removed from the molds for subsequent analysis.

Specimens for transmission electron microscopy (TEM) and transmission electron microtomography (TEMT) were prepared by cross-sectioning the bulk films obtained above at ambient temperature in a Reichert−Jung Ultracut-S ultramicrotome. The electron-transparent sections were picked up on copper TEM grids and exposed to the vapor of 2% RuO_4(aq) for 7 min to stain the phenyl rings of the DBS molecules.[22] Energy-filtered images were acquired with a Zeiss EM902 electron spectroscopic microscope operated at 80 kV and an energy loss of 0 eV. For TEMT, a series of 121 projections were collected along a single tilt axis from a specimen composed of 6.0 wt % DBS and 1.0 wt % CS at tilt angles ranging from +60 to −60° at an angular interval of 1° on a Technai T20 computerized transmission electron microscope operated at 200 kV. The images, acquired at a resolution of 1.50 nm/pixel, were aligned using 9 CS nanoparticles inherent in the sample as fiducial markers, rather than decorating the surface with Au colloidal beads. The average error encountered in aligning the images was 6.6%. Once aligned, the image set was reconstructed using the EMCAT software package[30] into a volume element according to the filtered (*r*-weighted) back-projection reconstruction algorithm.

Dynamic rheometry was performed on a Rheometrics Solids Analyzer (RSA II). The bulk films were trimmed to about 5 mm × 2.5 mm and analyzed in the film and fiber geometry. Frequency (ω) spectra of the dynamic elastic and viscous tensile moduli (E' and E'', respectively) were obtained at a strain amplitude of 0.003% (in the linear viscoelastic regime) from at least 10^0 to 10^2 rad/s, and temperature sweeps were performed at a rate of 1 °C/min at $\omega = 10$ Hz. Melt rheology was conducted at 100 °C on a Rheometrics Mechanical Spectrometer (RMS 800) using 8 mm parallel plates separated by a 1 mm gap. Circles measuring 8 mm in diameter were trimmed from the bulk films and placed between the parallel plates at ambient temperature and then heated to 100 °C to ensure good adhesion to the plates. Frequency spectra of the dynamic elastic and viscous shear moduli (G' and G'', respectively) were acquired at a strain of 5% (in the linear viscoelastic regime) from at least 10^0 to 10^2 rad/s.

Results and Discussion

Morphological Characteristics. Prior morphological studies of DBS networks in a wide variety of low-molar-mass organic solvents[31,32] and polymers[22,25,28] indicate that the nanofibrillar diameter can range substantially, from about 10 nm to 0.8 μm. In a companion study of DBS in PEG, we have demonstrated[24] that, while a single specimen may exhibit a broad range of nanofibrillar diameters, a primary unit measuring on the order of 9−11 nm in diameter appears to exist. Larger nanofibrillar elements may therefore represent aggregates or bundles of these primary nanofibrils or, alternatively, incompletely dissolved DBS. Another interesting feature of DBS nanofibrils is their branching. Thierry et al.[16,29] have shown that the nanofibrils formed in tetrahydrofuran/benzene solutions grow very long and exhibit surprisingly few branch points. In marked contrast, DBS networks in silicone polymers[25,28,33] and polyethers[24] can appear highly branched and interconnected, depending on DBS concentration and relevant matrix properties (e.g., polarity). Nanofibrillar branching constitutes an important consideration in the development of load-bearing skeletal networks and may likewise provide fundamental insight into the mechanism by which the nanofibrils form (e.g., by noncrystallographic branching[34]). The primary DBS nanofibrils intermittently exhibit several other interesting characteristics such as a rope-like helical pitch that measures on the order of 100 nm.[32] Recently, we have documented[24] a morphology suggesting that networked DBS nanofibrils may, in fact, be hollow tubes.

Figure 1 shows a series of TEM images of DBS nanofibrils in PEMA at DBS concentrations ranging from 0.5 to 7.0 wt % (the corresponding image obtained from neat PEMA is structureless and is not included here for that reason). Close examination of Figures 1a and 1b reveals the presence of very faint, but discrete, nanofibrils measuring about 10 nm across. The phenyl rings of the DBS molecules are selectively stained by RuO_4 and appear electron dense (dark) relative to the unstained PEMA background. It is interesting to note that DBS nanofibrils are more clearly evident at lower concentrations in polyethers to which DBS is melt-blended.[22,24] In the present

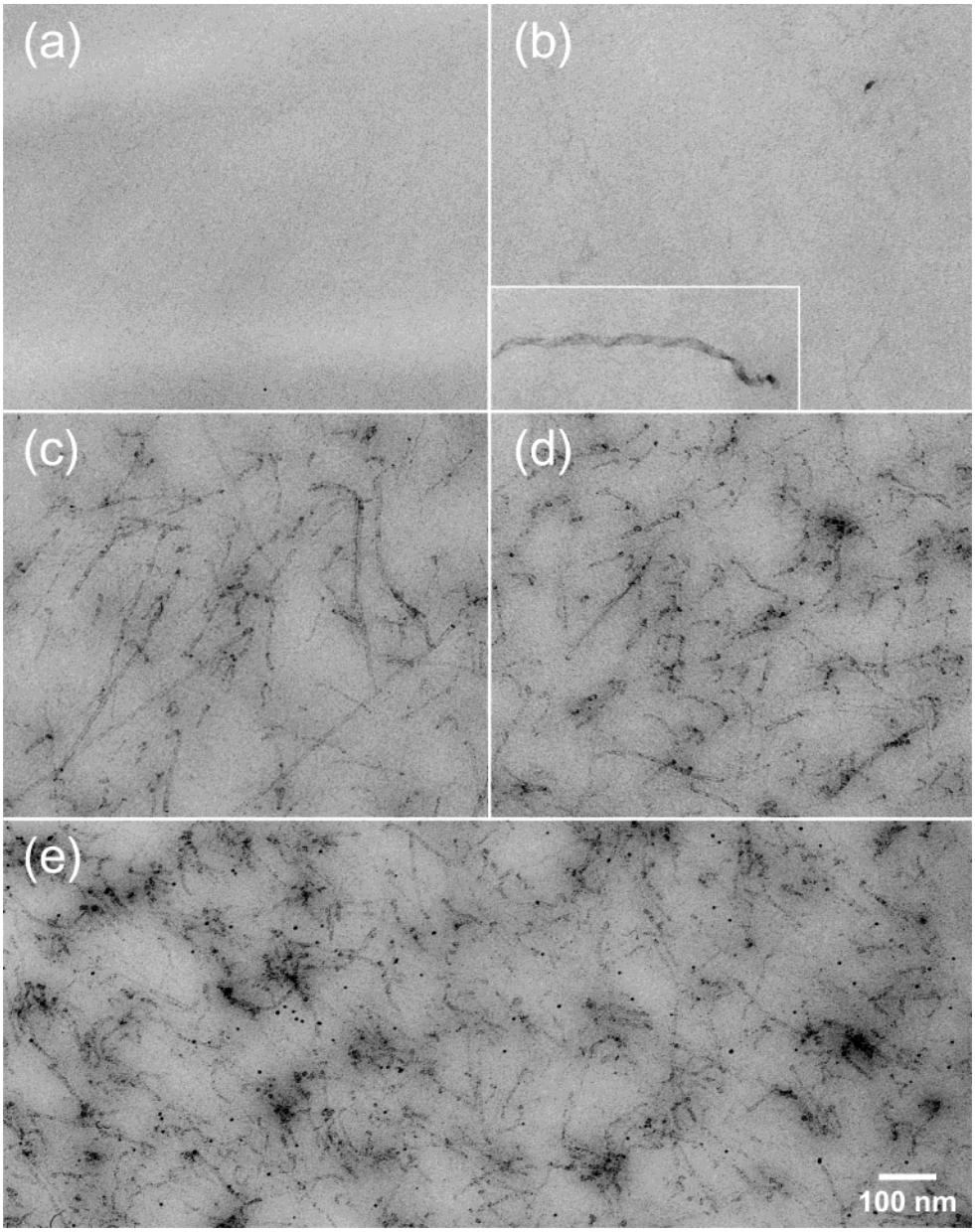

Figure 1. Zero-loss energy-filtered TEM images of PEMA/DBS formulations containing different DBS concentrations (in wt %): (a) 0.5, (b) 1.0, (c) 3.0, (d) 5.0 and (e) 7.0. In all cases, DBS nanostructural elements appear electron-opaque (dark) due to RuO_4 staining of the phenyl rings. The inset included in (b) shows an isolated DBS ribbon.

case, the DBS is co-dissolved with PEMA in acetone (to avoid thermal degradation of the PEMA at elevated temperatures), which may affect the kinetics by, or the extent to, which the DBS molecules self-organize. The inset of Figure 1b displays an isolated DBS ribbon discovered within the specimen. While relatively uncommon, supramolecular features such as this ribbon provide evidence of either incomplete DBS dissolution during specimen preparation (which is considered improbable under the conditions employed here) or extensive molecular organization of DBS due most likely to localized composition heterogeneities. As the DBS concentration is increased to 3.0 wt % and higher (Figures 1c−e), well-defined nanofibrils exhibiting random orientation become apparent. Even the speckles seen in these images can be sensibly interpreted as nanofibrils oriented parallel to the *z*-direction (i.e., the direction of the electron beam). Since the nanofibrils consistently measure ca. 10 nm in diameter, they are considered primary units, rather than aggregates or nanofibrillar bundles.

The images presented in Figure 1 confirm that the number density of nanofibrils increases with increasing DBS concentration, and an increase in number density is accompanied by a transition from single, unbranched nanofibrils up to 500 nm in length (Figure 1c) to a more compact, branched network morphology (Figure 1e). Relatively large, but discrete, electron-dense regions are clearly visible in Figure 1e and may be considered as loose aggregates that either formed upon solvent removal or never completely dissolved during specimen preparation. On the basis of the extent to which the nanofibrillar network is uniformly distributed in this and comparable images, we expect that these loose aggregates developed as the specimens dried. It is interesting to note that, while Mitra and Misra[35] used light scattering to establish the existence of DBS aggregates measuring ∼0.15 μm across in polystyrene and polycarbonate, they failed to recognize the propensity for DBS to self-organize into a fine nanofibrillar network. One final feature of Figure 1 warranting mention is that a large population

SCHEME 2

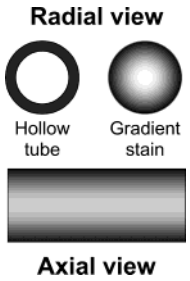

of the stained nanofibrils (particularly in Figure 1c) appears hollow. This feature, which becomes less pronounced with increasing DBS concentration and network formation, is strikingly reminiscent of results reported[24] for PEG/DBS organogels and can be interpreted to mean that either (*i*) the nanofibrils are tubular in nature and possess a hollow (non-DBS containing) core, or (*ii*) the RuO_4 stains only the peripheral phenyl rings of the DBS molecules, as depicted in Scheme 2. Recent efforts by Terech and Talmon[36] have established that some gel networks do, in fact, consist of nanoscale tubules. Although it is not possible to distinguish between these possibilities from Figure 1, we can immediately eliminate the possibility of stained polymer bound to the nanofibrillar surface, as previously proposed[24] as a third option to explain this morphological curiosity.

The image series displayed in Figure 2 is obtained from PEMA/CS nanocomposites containing 1.0 wt % CS with DBS concentrations ranging from 0.0 to 6.0 wt % (corresponding to 1.0 to 7.0 wt % additive content). As expected from their composition, the CS nanoparticles alone appear electron dense (see Figure 2a) and range in diameter from about 10 to 20 nm, in favorable agreement with the characterization data provided by the manufacturer. Addition of 1.0 wt % DBS to the PEMA/CS nanocomposite promotes the formation of the ill-defined nanofibrils seen in Figure 2b. By increasing the DBS concentra-

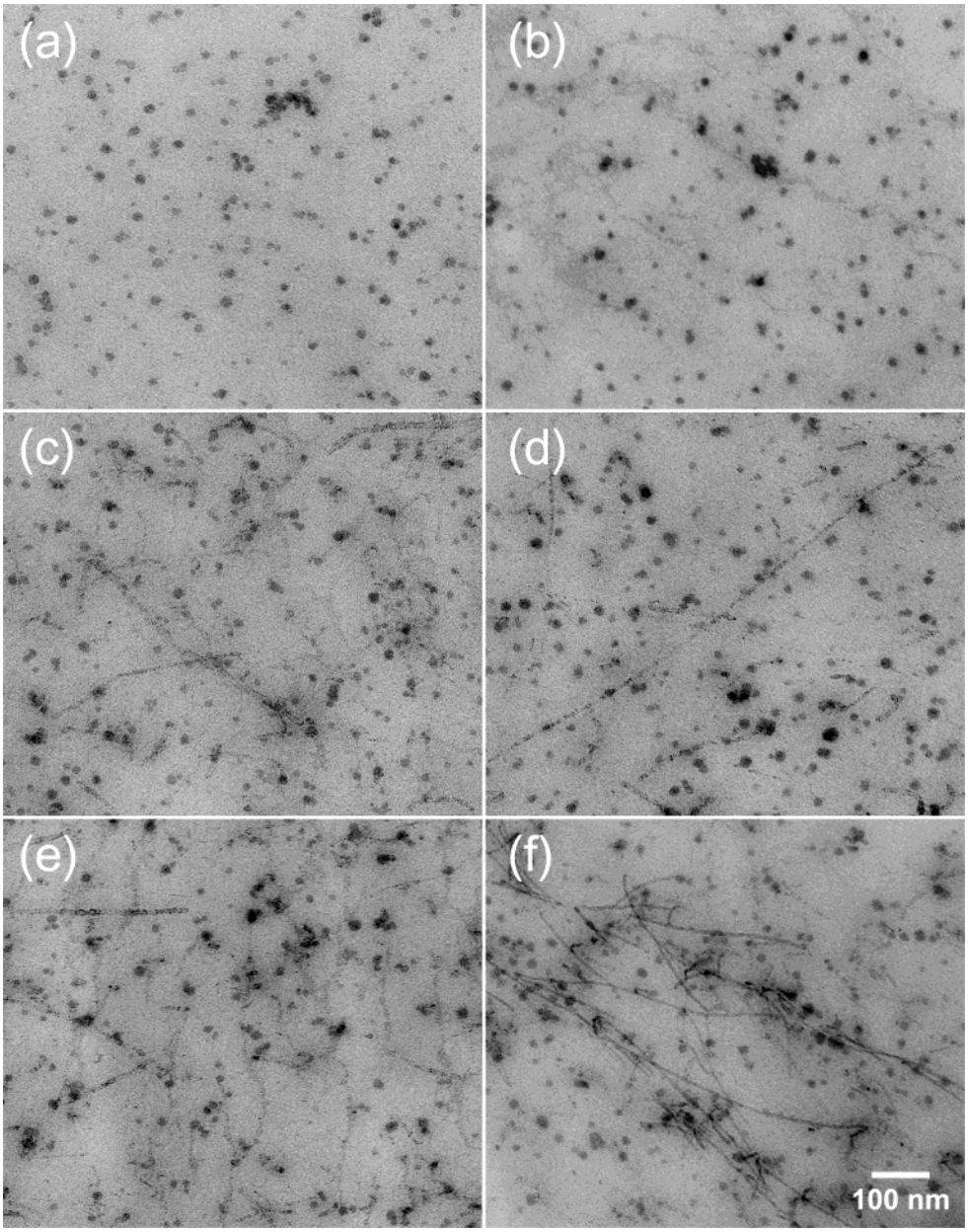

Figure 2. Energy-filtered TEM images of PEMA/DBS/CS nanocomposites containing 1.0 wt % CS and different DBS concentrations (in wt %): (a) 0.0, (b) 1.0, (c) 3.0, (d) 4.0, (e) 5.0, and (f) 6.0. The CS nanoparticles measure about 20 nm on average and, as siliceous media, appear dark relative to the PEMA matrix due to their composition. As in Figure 1, DBS nanofibrils likewise appear dark due to selective staining.

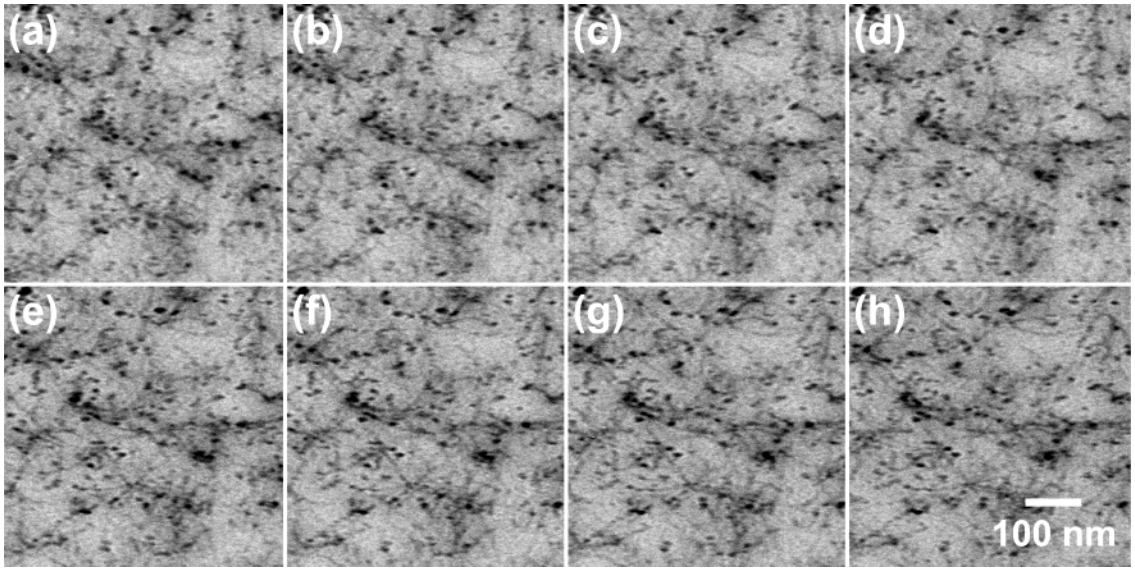

Figure 3. Sequential series of TEM tilt projections collected from a 93/6/1 w/w PEMA/DBS/ CS nanocomposite and aligned with regard to the CS nanoparticles present in the material. The angular increment between adjacent images is constant at 5° so that they can be viewed as stereopairs, which permit direct visualization of the 3D nature of the morphology.

tion, the nanofibrils become better defined, measuring ~10 nm in diameter, and eventually show signs of network development at DBS concentrations of 5.0 wt % and higher. Included in Figure 2 is an image acquired from a 93/6/1 w/w PEMA/DBS/ CS nanocomposite (Figure 2f) that reveals exceptionally well-defined, unbranched nanofibrils. While this particular formulation generally tends to exhibit a morphology that more closely resembles that shown in Figure 2e for the nanocomposite with 5.0 wt % DBS, isolated patches exhibit this markedly different morphology, the origin of which is not yet fully understood. Scrutinization of all the images displayed in Figure 2 confirms that some, but not many, of the DBS nanofibrils likewise appear peripherally stained, in which case they may in fact be tubular.

The morphologies of the PEMA/DBS/CS nanocomposites are clearly complex when viewed as 2D projections. Insightful features such as the extent of nanofibrillar branching, as well as evidence for interaction between CS nanoparticles and DBS nanofibrils, simply cannot be gleaned from such images with any degree of certainty. To explore these issues in more detail, we have performed TEMT on the nanocomposite with the highest additive loading level (93/6/1 w/w PEMA/DBS/CS). This methodology has been recently and successfully used[37−40] to discern and quantitate the local and global topologies of complex block copolymer morphologies. The TEMT procedure requires a large set of images collected from a single specimen at a regular tilt interval.[41] A subset of the images collected here for this purpose is presented in 5° increments (to permit stereopair viewing) in Figure 3. The 1024 × 1024 pixel images acquired during the course of this study are too large for display purposes, and so only a portion of these images is shown in Figure 3. Close examination of these images reveals how the orientation and apparent connectivity of the nanofibrils present change upon tilting. The quality of alignment can be determined explicitly from the angle-dependent mean positional error ($\langle\Delta\rangle$), where Δ is the difference between measured and calculated positions of each reference particle at each tilt angle (θ).[37] Values of $\langle\Delta\rangle$, discerned by averaging the individual Δ values obtained for the 9 fiducial particles employed in the alignment, are presented as a function of θ in Figure 4 and confirm that the θ-averaged mean error incurred during image alignment is considerably less (19%) than the spatial resolution of the images.

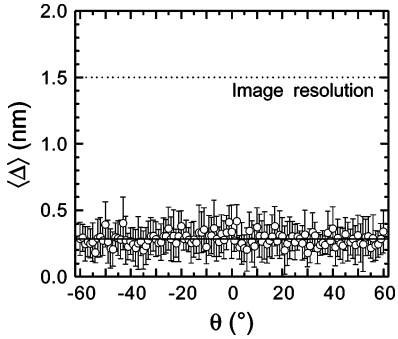

Figure 4. Mean positional error ($\langle\Delta\rangle$) of the reference markers used to align 121 tilt images (such as those displayed in Figure 3) presented as a function of tilt angle (θ). The error bars represent the standard deviation in the data, and the solid and dashed lines identify the θ-averaged $\langle\Delta\rangle$ and image resolution, respectively.

Once the images are accurately aligned, application of the filtered back-projection reconstruction algorithm renders a 3D volume element that can be sliced along any orthogonal direction. The image series provided in Figure 5 represents a small subset of 2D slices extracted from the 3D volume element along the *z*-axis.

Each slice in Figure 5 corresponds to 1.5 nm along the *z*-direction and therefore contains precisely 1.5 nm of information (which would be unobtainable by any other analytical means). Sequential images displayed in this series are separated by 4 slices (6.0 nm), which corresponds to about half the nanofibrillar diameter deduced earlier. Nanofibrillar diameters are more reliably measured from images such as these (since overlap is completely eliminated) and range from 8 to 12 nm. In addition to the local nanofibrillar orientation, two other features can be gleaned from this series of 2D slices. The first is that the series traverses the entire TEM section, since the specimen surface is encountered in the first and last images. From this observation, the specimen thickness is estimated to be on the order of 60 nm, which agrees well with the setting of the ultramicrotome. Moreover, the specimen appears slightly tilted relative to the *z*-axis, since the surfaces (dis)appear from view gradually. Thus, we can conclude that the TEM section was not lying flat on the grid during image acquisition. Slices

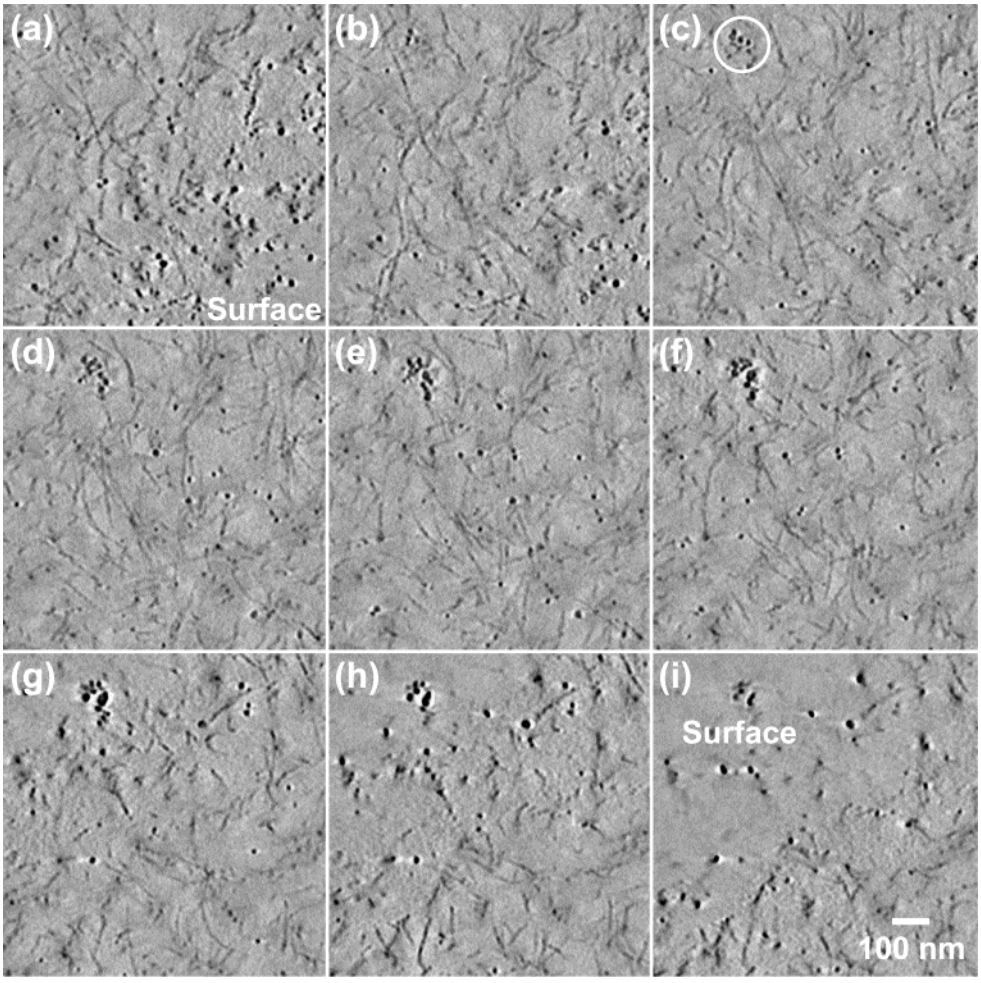

Figure 5. Sequence of TEMT slices of the 93/6/1 w/w PEMA/DBS/CS nanocomposite extracted from a complete 3D reconstruction of serial tilt projections, such as those displayed in Figure 3, by the filtered (*r*-weighted) back-projection procedure. Each image corresponds to a thickness of 1.5 nm, and adjacent images are separated by 6.0 nm along the *z*-axis, which is parallel to the electron beam. The upper and lower surfaces of the TEM specimen are identified, as is a cluster of CS nanoparticles (which appears in several images).

in close proximity to either surface indicate that the nanofibrils reside near the PEMA surface upon casting from acetone, in which case they may therefore be considered uniformly distributed throughout the polymer matrix. The CS nanoparticles, on the other hand, appear to enrich one of the surfaces (compare Figures 5a and 5i), the identity of which (PEMA/Teflon or PEMA/air) cannot be directly discerned from these data.

Another enlightening feature of several images in Figure 5 is that the DBS nanofibrils originate/terminate in close proximity to a CS nanoparticle, suggesting a physical interaction between the two species. Since DBS molecules interact and self-organize into nanofibrils primarily through hydrogen bonding and π phenyl interactions,[17] it would not be altogether surprising that DBS molecules hydrogen-bond to CS nanoparticles containing surface hydroxyl groups. If this is the case, then the DBS nanofibrils might be heterogeneously seeded (nucleated) by the CS nanoparticles, which would explain the difference in nanofibrillar morphologies evident in Figures 1 and 2. Moreover, the nanofibrils could serve to stabilize the CS nanoparticles and hinder undesirable large-scale aggregation (which would ultimately affect the optical clarity of PEMA if sufficiently widespread). To discern the quality of the reconstruction and, hence, the slices presented in Figure 5, the slices generated from the reconstructed 3D volume element can be stacked and combined by the NIH Image software package to yield an average (composite) projection that should appear similar to that acquired by conventional TEM. A portion of the average image produced in this fashion is shown in Figure 6 and corroborates that the morphology of this PEMA/DBS/CS nanocomposite is comparable to those displayed in Figure 2. To facilitate comparison between Figures 5 and 6, a CS nanoparticle aggregate is identified in both image sets. Several 3D images of portions of the volumetric reconstruction used to generate Figures 5 and 6 are provided in Figure 7 to illustrate the spatial relationship between the DBS nanofibrils and the CS nanoparticles at relatively high magnification. Of particular interest here are nanofibrillar junctions, termini, and orientation, since these features are not readily discernible from conventional 2D TEM projections.

Mechanical Properties. To ascertain the effect of the DBS nanofibrils on the bulk properties of PEMA, several mechanical tests have been performed. The ambient-temperature frequency (ω) spectra of the dynamic elastic tensile modulus (E') of PEMA/DBS specimens differing in composition are provided in Figure 8 and clearly indicate that the magnitude of E' is not sensitive to DBS concentration over the range explored in this work. Although the morphological analysis unambiguously reveals the existence of nanofibrils throughout the PEMA matrix, this result strongly suggests that the nanofibrils have virtually no effect on the mechanical properties of glassy PEMA. Previous X-ray diffraction data have confirmed[22] that the DBS nanofibrils (procured from solvent-extracted organogels) are at

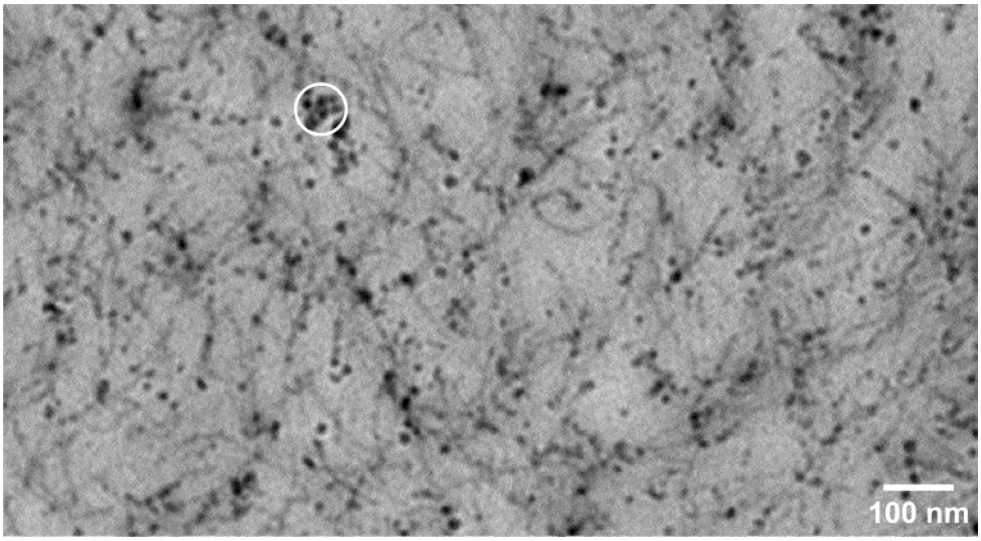

Figure 6. An average (composite) image of the 93/6/1 w/w PEMA/DBS/CS nanocomposite generated by combining all the TEMT slices produced during the 3D reconstruction. The circled CS cluster provides a reference point for comparison with the slices provided in Figure 5.

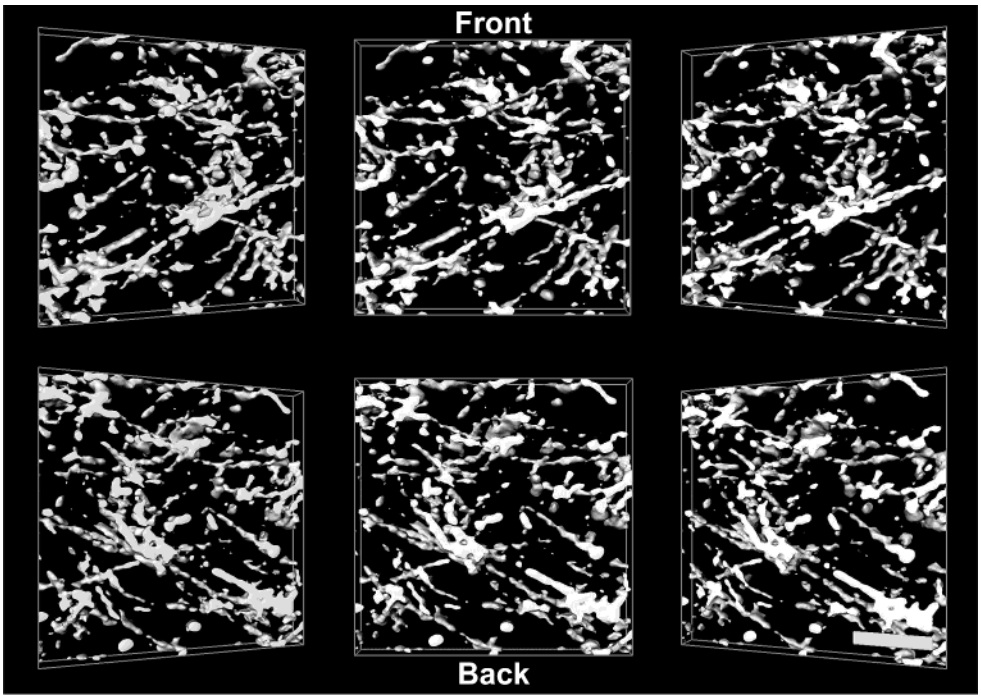

Figure 7. Three-dimensional visualizations of a small portion measuring 375 × 375 × 27 nm of the volumetric reconstruction used to generate Figures 5 and 6. These images show the front and back of the reconstruction, as well as oblique views at ±15°, and illustrate the spatial arrangement of the DBS nanofibrils and CS nanoparticles relative to each other in the 93/6/1 PEMA/DBS/CS nanocomposite. The scalemarker provided in the lower right image corresponds to 100 nm.

least partially crystalline. Since an increase in polymer crystallinity can have a modest (although often negligible) effect on E' below T_g,[42] a slight concentration-dependent increase in E' might be anticipated in the present systems. Recall that, in the glassy state, the motion of the PEMA molecules is highly restricted. The presence of a DBS crystalline nanostructure may serve to restrict chain mobility further, thereby promoting a slight, if detectable, increase in E'. Although they are presumably crystalline, the DBS nanofibrils are not, however, expected to reduce the mobility of vitrified chains and, in light of this consideration, E' to an appreciable level, which is consistent with the results presented here. One last noteworthy feature of the ω spectra in Figure 8 is that the variation in E' varies from about 25 to 50%, which implies that this ω dependence, albeit slight, is most likely real and not within the experimental uncertainty of the measurements. As discussed further below, Fahrländer et al.[23] have reported a comparably weak dependence of the dynamic elastic shear modulus (G') on ω in PPG/DBS organogels.

In marked contrast, the addition of DBS to PEMA is found to influence the magnitude of E' at temperatures just above T_g in the melt. Figure 9a shows the dependence of E' on temperature for specimens containing up to 7.0 wt % DBS. [Note that the $E'(T)$ data collected from the system with 1.0 wt % DBS closely resemble those of neat DBS and are not included here for that reason.] As seen in Figure 8, E' is not dependent (within experimental uncertainty) on DBS composition below the T_g of PEMA (measured to be 85 °C from the temperature

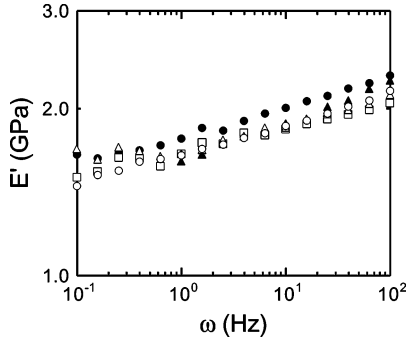

Figure 8. Dependence of the dynamic elastic modulus (E') on frequency (ω) for PEMA/DBS systems containing different DBS concentrations (in wt %): 0.0 (○), 1.0 (□), 3.0 (●), 5.0 (△), and 7.0 (▲). The strain amplitude is 0.003%, and the temperature is 25 °C.

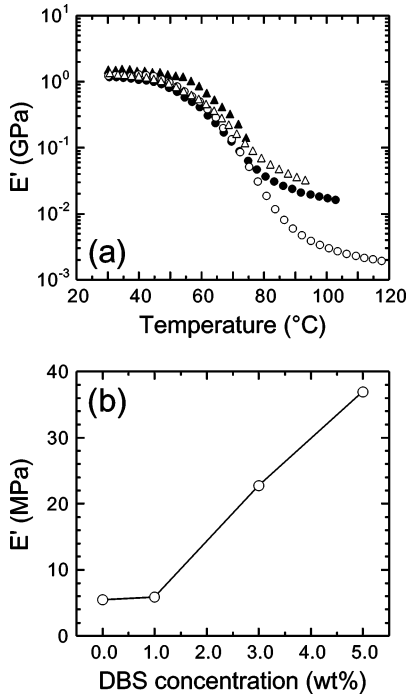

Figure 9. In (a), the temperature dependence of E' for PEMA/DBS systems with different DBS concentrations (in wt %): 0.0 (○), 3.0 (●), 5.0 (△), and 7.0 (▲). The heating rate is constant at 1 °C/min, and the frequency is 10 Hz. In (b), values of E' evaluated at 90 °C are presented as a function of DBS concentration. The solid line in (b) serves to connect the data.

dependence of tan δ, where tan $\delta = E''/E'$, in contrast to the manufacturer's reported value of 63 °C). It is therefore unlikely that the PEMA matrix is plasticized due to residual solvent. Addition of up to 5 wt % DBS results in a ~10 °C reduction in the PEMA T_g, which implies that molecularly dissolved DBS remains in the PEMA matrix (up to its solubility limit) even after some fraction of the DBS molecules self-organize into nanofibrils. Moreover, the temperature range over which reliable $E'(T)$ data could be reproducibly collected is found to decrease systematically, suggesting that the DBS-modified PEMA becomes increasingly brittle, as the concentration of DBS is increased. At temperatures above T_g, however, the magnitude of E' tends to increase with increasing DBS concentration, indicating that the DBS nanofibrils are stiff (which is consistent with the presumption that they are at least partially crystalline) and are therefore more capable of supporting a load than the molten PEMA matrix. It is interesting to recognize that at DBS

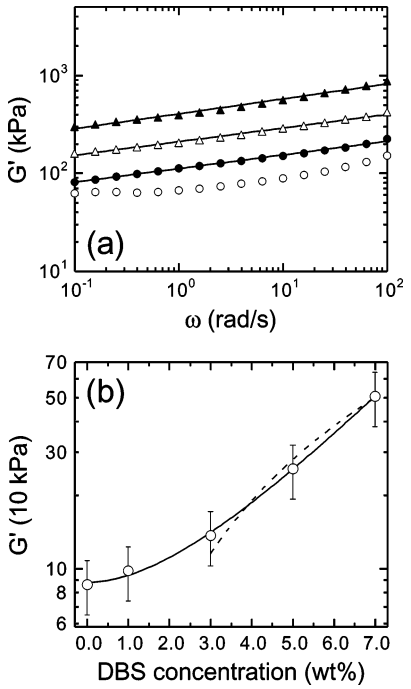

Figure 10. In (a), frequency spectra of the dynamic elastic modulus (G') measured at 100 °C for PEMA/DBS melts containing different DBS concentrations (in wt %): 0.0 (○), 3.0 (●), 5.0 (△), and 7.0 (▲). The solid lines denote power-law fits to three of the four data sets obtained at a strain amplitude of 5%. In (b), average values of G' determined from the ω spectra in (a) are shown as a function of DBS concentration. The solid line serves as a guide for the eye, while the dashed line represents a power-law fit to the data over the DBS concentration range corresponding to network formation in Figure 1. The error bars denote one standard deviation in the data.

concentrations below that required to form a network (see Figure 1), E' is virtually unaffected by the addition of DBS at $T > T_g$. At higher concentrations, Figure 9b reveals that E' increases almost linearly with increasing DBS content.

To probe this concentration effect in more detail, polymer melt rheology has been performed on PEMA/DBS systems with up to 7.0 wt % DBS. Figure 10a displays the ω spectra of the dynamic elastic shear modulus (G') acquired at 100 °C for several different formulations. While G' exceeds its dynamic viscous analogue (G'') over the entire range of ω explored, these spectra suggest that G' is a function of ω, which is contrary to the prerequisite that G' must be independent of ω (especially at low ω) for a material to be classified as a gel.[43] The variation in G' from 10^{-1} to 10^{2} rad/s is in excess of 250%, confirming that this ω dependence is not due to experimental uncertainty. Analysis of these $G'(\omega)$ data reveals a common scaling relationship of the form $G' \sim \omega^{0.14}$ for those specimens containing DBS. This observation is intriguing, since Fahrländer et al.[23] report a similar ω-dependent relationship, with a universal exponent of 0.05, for organogels composed of PPG and DBS. Another salient feature of Figure 10a is the dependence of G' on DBS concentration, which is explicitly shown in Figure 10b and which confirms that G' (averaged over the ω range examined) increases with increasing DBS content. At DBS concentrations corresponding to network morphologies in Figure 1, G' scales with respect to DBS content. Although a very limited concentration range is sampled (3.0 to 7.0 wt % in Figure 10b), we find it intriguing that the scaling exponent is 1.7, which agrees surprisingly well with that measured[24] from PEG/DBS organogels over a much broader concentration range. Such agreement implies that G' provides a direct measure of DBS

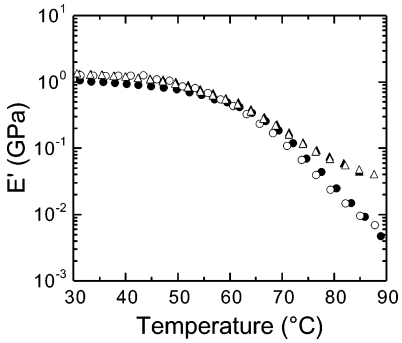

Figure 11. The dynamic elastic modulus (E') presented as a function of temperature for PEMA (○), PEMA with 5.0 wt % DBS (△), a PEMA/CS nanocomposite with 1.0 wt % CS (●) and the same nanocomposite with 5.0 wt % DBS (▲).

network morphology,[44] which can be controllably varied by concentration and solvent polarity.

Addition of 1.0 wt % CS to PEMA and PEMA/DBS mixtures has very little effect on the low-strain mechanical properties of these nanocomposite systems at temperatures below T_g and no discernible effect at all on the PEMA T_g determined from tan δ. The dependence of E' on temperature is displayed in Figure 11 for PEMA/CS nanocomposites with and without 5.0 wt % DBS. Although siliceous nanofillers have been previously reported to improve the mechanical properties of polymers such as poly(ethylene glycol),[10] poly(dimethylsiloxane) and poly(*n*-butylamino thionylphosphazene),[7] all the data sets in this figure appear virtually indistinguishable at low temperatures. As the temperature is increased above T_g, however, the CS increases E' slightly, but not as much as the DBS. Under these conditions, inclusion of 1.0 wt % CS in the PEMA/DBS formulation does not promote any discernible improvement in E' beyond that attained by DBS alone. While the DBS-induced increase in melt modulus will undoubtedly affect melt processing conditions by increasing the apparent (or complex) viscosity, it can also be envisaged as an effective means by which to extend the application range of PEMA and its nanocomposites. Another property that should be at least briefly addressed here is optical clarity, since this a generally important characteristic of acrylic polymers. Despite up to 7.0 wt % additive (DBS and/or DBS + CS), the PEMA/DBS formulations and PEMA/DBS/CS nanocomposites examined during the course of this work remain optically clear with no perceivable change in clarity, as evidenced by the photographic comparison presented in Figure 12. This observation differs markedly from results reported for DBS in other polymeric matrices. In polyethers and their copolymers, for instance, DBS molecules self-organize into macroscopic spherulites that induce opacity at lower concentrations.[22,23,27,28] Retention of transparency indicates that the DBS nanofibrillar network/aggregates and CS aggregates remain sufficiently small and dispersed at relatively high concentrations to avoid diffracting visible light.

Conclusions

The self-organization ability of organic gelators such as DBS motivates the development of multifunctional polymeric materials possessing nanoscale networks,[45] as well as the ongoing desire to control the morphology and connectivity of such networks.[46] Previous studies of DBS in a variety of polymers have established that DBS spontaneously orders into nanofibrils and, at sufficiently high concentrations, elastic networks capable of inducing physical gelation. In this work, we have investigated

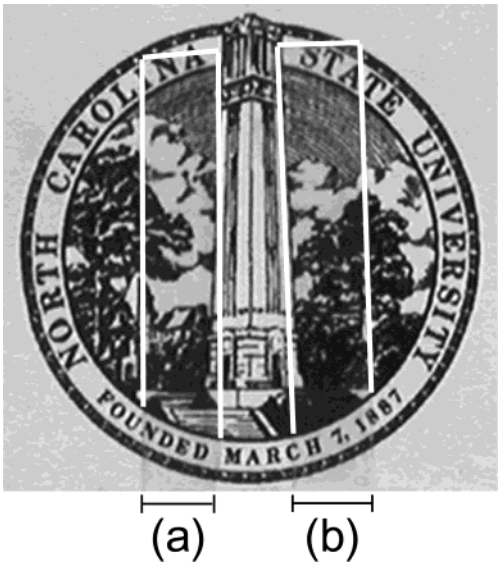

Figure 12. Photographs of (a) a pure PEMA film and (b) a PEMA film containing 6.0 wt % DBS and 1.0 wt % CS. The film thicknesses are comparable (ca. 100 μm). No discernible change in optical clarity is apparent from this comparison.

the self-organization efficacy of DBS in a glassy polymer and the effect of nanostructural formation on the corresponding mechanical properties. Morphological analysis of PEMA/DBS systems demonstrates that, at low DBS concentrations, the DBS nanofibrils are, for the most part, ill-defined. As the concentration of DBS is increased, however, TEM images confirm the development of discrete and networked nanofibrils measuring about 10 nm in diameter. A similar trend is observed upon addition of CS to produce a hybrid polymer nanocomposite. Three-dimensional information has been extracted from one such nanocomposite by TEMT, which (*i*) reveals a uniform distribution of DBS nanofibrils in the PEMA matrix, and (*ii*) provides evidence for physical interaction between DBS and CS during specimen preparation. Despite its formation into well-defined nanofibrils, DBS has no discernible effect on the elastic modulus of glassy PEMA. As the temperature is elevated above T_g, however, the existence of a nanostructure becomes evident, with the modulus increasing systematically with DBS concentration. Although 1.0 wt % CS has no effect on the properties of PEMA and PEMA/DBS systems at both ambient and elevated temperatures, higher concentrations will eventually promote mechanical property changes in PEMA, and the incorporation of DBS may help to disperse such nanoparticles and ultimately stabilize organic/inorganic nanocomposites.

Acknowledgment. E.A.W. is grateful to the Eastman Chemical Co. and the North Carolina Space Grant Consortium for graduate research fellowships. D.A.A. and M.B.B. are supported by the National Institutes of Health. H.J. is grateful to the Nanostructure Polymer Project supported by the New Energy and Industrial Technology Development Organization. We thank T. Kaneko for technical assistance.

References and Notes

(1) Osaheni, J. A.; Truby, K. E.; Silvi, N. *Macromol. Symp.* **2001**, *169*, 261.

(2) Sidorov, S. N.; Volkov, I. V.; Davankov, V. A.; Tsyurupa, M. P.; Valetsky, P. M.; Bronstein, L. M.; Karlinsky, R.; Zwanziger, J. W.; Matveeva, V. G.; Sulman, E. M.; Lakina, N. V.; Wilder, E. A.; Spontak, R. J. *J. Am. Chem. Soc.* **2001**, *123*, 10502.

(3) Coronado, E.; Galan-Mascaros, J. R.; Gomez-Garcia, C. J.; Laukhin, V. *Nature* **2000**, *408*, 447.
(4) Croce, F.; Appetecchi, G. B.; Persi, L.; Scrosati, B. *Nature* **1998**, *394*, 456.
(5) Winiarz, J. G.; Zhang, L. M.; Lal, M.; Friend, C. S.; Prasad, P. N. *J. Am. Chem. Soc.* **1999**, *121*, 5287.
(6) Wang, Y.; Herron, N. *Science* **1996**, *273*, 632.
(7) Lu, X.; Manners, I.; Winnik, M. A. *Macromolecules* **2001**, *34*, 1917.
(8) Patel, N. P.; Miller, A. C.; Spontak, R. J. *Adv. Mater.* **2003**, *15*, 729.
(9) MacLachlan, M. J.; Ginzburg, M.; Coombs, N.; Raju, N. P.; Greedan, J. E.; Ozin, G. A.; Manners, I. *J. Am. Chem. Soc.* **2000**, *122*, 3878.
(10) Walls, H. J.; Riley, M. W.; Singhal, R. R.; Spontak, R. J.; Fedkiw, P. S.; Khan, S. A. *Adv. Funct. Mater.* **2003**, *13*, 710.
(11) Forsyth, M.; MacFarlane, D. R.; Best, A.; Adebahr, J.; Jacobsson, P.; Hill, A. J. *Solid State Ionics* **2002**, *147*, 203.
(12) Merkel, T. C.; Freeman, B. D.; Spontak, R. J.; He, Z.; Pinnau, I.; Meakin, P.; Hill, A. J. *Science* **2002**, *296*, 519.
(13) Watase, M.; Itagaki, H. *Bull. Chem. Soc. Jpn.* **1998**, *71*, 1457.
(14) Sterzynski, R.; Lambla, M.; Crozier, H. *Adv. Polym. Technol.* **1994**, *13*, 25.
(15) Angyal, S. J.; Lawler, J. V. *J. Am. Chem. Soc.* **1944**, *66*, 837.
(16) Thierry, A.; Fillon, B.; Straupé, C.; Lotz, B.; Wittmann, J. C. *Prog. Colloid Polym. Sci.* **1992**, *87*, 28.
(17) Wilder, E. A.; Spontak, R. J.; Hall, C. K. *Mol. Phys.*, in press.
(18) Thomas, P.; Sibi, S. *Comptes Rendus* **1926**, *183*, 282.
(19) Yamamoto, S. *Kougyou Kagaku Zasshi* **1942**, *45*, 695.
(20) Kobayashi, T.; Hasegawa, H.; Hashimoto, T. *Nihon Reoroji Gakkaishi* **1989**, *17*, 155.
(21) Mercurio, D. J.; Khan, S. A.; Spontak, R. J. *Rheol. Acta* **2001**, *40*, 30.
(22) Mercurio, D. J.; Spontak, R. J. *J. Phys. Chem. B* **2001**, *105*, 2091.
(23) Fahrländer, M.; Fuchs, K.; Friedrich, C. *J. Rheol.* **2000**, *44*, 1103.
(24) Wilder, E. A.; Hall, C. K.; Khan, S. A.; Spontak, R. J. *Langmuir* **2003**, *19*, 600.
(25) Ilzhoefer, J. R.; Spontak, R. J. *Langmuir* **1995**, *11*, 3288.
(26) Janssen, R. H. C.; Stümpflen, V.; van Boxtel, M. C. W.; Bastiaansen, C. W. M.; Broer, D. J.; Tervoort, T. A.; Smith, P. *Macromol. Symp.* **2000**, *154*, 117.
(27) Wilder, E. A.; Hall, C. K.; Spontak, R. J. *J. Colloid Interface Sci.*, in press.
(28) Ilzhoefer, J. R.; Broom, B. C.; Nepa, S. M.; Vogler, E. A.; Khan, S. A.; Spontak, R. J. *J. Phys. Chem.* **1995**, *99*, 12069.
(29) Thierry, A.; Straupé, C.; Lotz, B.; Wittmann, J. C. *Polym. Commun.* **1990**, *31*, 299.
(30) Fung, J.; Liu, W.; Ruijter, W. J. D.; Chem, H.; Abbey, C. J.; Sedat, J. W.; Agard, D. R. *J. Struct. Biol.* **1996**, *116*, 181.
(31) Yamasaki, S.; Tsutsumi, H. *Bull. Chem. Soc. Jpn.* **1994**, *67*, 906.
(32) Yamasaki, S.; Tsutsumi, H. *Bull. Chem. Soc. Jpn.* **1995**, *68*, 123.
(33) Smith, J. M.; Katsoulis, D. E. *J. Mater. Chem.* **1995**, *5*, 1899.
(34) Liu, P.; Sawant, P. D. *Adv. Mater.* **2002**, *14*, 421.
(35) Mitra, D.; Misra, A. *Polymer* **1988**, *29*, 1990.
(36) Terech, P.; Talmon, Y. *Langmuir* **2002**, *18*, 7240.
(37) Spontak, R. J.; Fung, J. C.; Braunfeld, M. B.; Sedat, J. W.; Agard, D. A.; Kane, L.; Smith, S. D.; Satkowski, M. M.; Ashraf, A.; Hajduk, D. A.; Gruner, S. M. *Macromolecules* **1996**, *29*, 4494.
(38) Laurer, J. H.; Hajduk, D. A.; Fung, J. C.; Sedat, J. W.; Smith, S. D.; Gruner, S. M.; Agard, D. A.; Spontak, R. J. *Macromolecules* **1997**, *30*, 3938.
(39) Jinnai, H.; Nishikawa, Y.; Spontak, R. J.; Smith, S. D.; Agard, D. A.; Hashimoto, T. *Phys. Rev. Lett.* **2000**, *84*, 518.
(40) Jinnai, H.; Nishikawa, Y.; Ito, M.; Smith, S. D.; Agard, D. A.; Spontak, R. J. *Adv. Mater.* **2002**, *14*, 1615.
(41) Frank, J. *Electron Tomography*; Plenum Press: New York, 1992.
(42) Ward, I.; Hadley, D. W.; Ward, A. M. *An Introduction to the Mechanical Properties of Solid Polymers*; Wiley and Sons: New York, 1993.
(43) Kavanagh, G. M.; Ross-Murphy, S. B. *Prog. Polym. Sci.* **1998**, *23*, 533.
(44) Torquato, S. *Random Heterogeneous Materials: Microstructure and Macroscopic Properties*; Springer-Verlag: New York, 2002.
(45) Terech, P.; Weiss, R. G. *Chem. Rev.* **1997**, *97*, 3133.
(46) Liu, X. Y.; Sawant, P. D.; Tan, W. B.; Noor, I. B. M.; Pramesti, C.; Chen, B. H. *J. Am. Chem. Soc.* **2002**, *124*, 15055.